J. Fluid Mech. (1998), *vol.* 362, *pp.* 1–15. Printed in the United Kingdom

Stability of wall modes in a flexible tube

By V. KUMARAN

Department of Chemical Engineering, Indian Institute of Science, Bangalore 560 012, India

(Received 24 January 1997 and in revised form 12 November 1997)

The asymptotic results (Kumaran 1998*b*) obtained for $\Lambda \sim 1$ for the flow in a flexible tube are extended to the limit $\Lambda \ll 1$ using a numerical scheme, where Λ is the dimensionless parameter $Re^{1/3}(G/\rho V^2)$, $Re = (\rho VR/\eta)$ is the Reynolds number, ρ and η are the density and viscosity of the fluid, R is the tube radius and G is the shear modulus of the wall material. The results of this calculation indicate that the least-damped mode becomes unstable when Λ decreases below a transition value at a fixed Reynolds number, or when the Reynolds number increases beyond a transition value at a fixed Λ. The Reynolds number at which there is a transition from stable to unstable perturbations for this mode is determined as a function of the parameter $\Sigma = (\rho GR^2/\eta^2)$, the scaled wavenumber of the perturbations kR, the ratio of radii of the wall and fluid H and the ratio of viscosities of the wall material and the fluid η_r. For $\eta_r = 0$, the Reynolds number at which there is a transition from stable to unstable perturbations decreases proportional to $\Sigma^{1/2}$ in the limit $\Sigma \ll 1$, and the neutral stability curves have a rather complex behaviour in the intermediate regime with the possibility of turning points and isolated domains of instability. In the limit $\Sigma \gg 1$, the Reynolds number at which there is a transition from stable to unstable perturbations increases proportional to Σ^{α}, where α is between 0.7 and 0.75. An increase in the ratio of viscosities η_r has a complex effect on the Reynolds number for neutrally stable modes, and it is observed that there is a maximum ratio of viscosities at specified values of H at which neutrally stable modes exist; when the ratio of viscosities is greater than this maximum value, perturbations are always stable.

1. Introduction

Many biological systems and biotechnology processes involve flow through flexible tubes and channels. The flow of blood and other fluids in the body takes place through flexible tubes, and the separation and purification processes in pharmaceutical industries often involve flow in tubes and channels made up of polymer matrices and membranes. These have been analysed using models similar to those for the flow in a rigid tube, but some experiments conducted by Krindel & Silberberg (1979) suggest that the characteristics of the flow in a flexible tube could be very different. The drag force in a flexible tube is much larger than that in a rigid tube of the same radius at Reynolds numbers where the flow in a rigid tube is laminar, and the anomalous drag force could not be accounted for by changes in the radius of the tube. This led them to conclude that the Reynolds number at which the flow changes from the laminar to turbulent regime is much smaller than the transition Reynolds number $Re = 2300$–4000 for a rigid tube, and the transition Reynolds number is influenced by the elasticity of the surface. It is useful, from a technological viewpoint, to develop a fundamental understanding of the factors affecting this transition, since this would

help in optimizing the design of biotechnological processes. In applications where it is important to have high mass or heat transfer rates, it would be necessary to operate the system in the turbulent regime where the transfer rates are up to three orders of magnitudes higher than that in the laminar regime. In processes where low drag forces are desirable, the system could be operated in the laminar regime.

At the point of transition from the laminar to turbulent regime, the laminar flow becomes unstable to small perturbations, and so it is necessary to study the stability characteristics of the flow to predict the Reynolds number at which there is a transition from stable to unstable modes. The stability of the 'viscous modes' in the flow through a flexible tube in the low Reynolds number regime, where $Re \equiv (\rho V R/\eta) \ll 1$, and $(V\eta/GR) \sim 1$ was analysed by Kumaran (1995*a*). Here, ρ and η are the density and viscosity of the fluid, R is the radius of the tube, V is the characteristic fluid velocity and G is the shear modulus of the wall material. In this regime, there is a balance between the viscous forces in the fluid and the elastic forces in the wall. It was observed that the viscous modes become unstable when the fluid velocity is increased beyond a critical value. The continuation of the viscous modes into the intermediate Reynolds number regime was analysed using a numerical solution scheme by Kumaran (1998*a*). The stability of the 'inviscid modes' in the high Reynolds number regime $Re \gg 1$ and $(\rho V^2/G) \sim 1$ was analysed using asymptotic techniques by Kumaran (1995*b*). In this case, there is a balance between the inertial forces in the fluid and the elastic forces in the wall, and the analysis indicated that the inviscid modes are always stable. The stability of 'wall modes' in the high Reynolds number regime $Re \gg 1$ and $Re^{1/3}(G/\rho V^2) \sim 1$, where the vorticity is confined to a small region of thickness $Re^{-1/3}$, was studied using asymptotic analysis in Kumaran (1998*b*). The results of that analysis showed that the wall modes are always stable in the limit of high Reynolds number. Here, the asymptotic results obtained in the limit of high Reynolds number are extended to the intermediate Reynolds number regime using numerical analysis, and it is found that the wall modes do become unstable in this regime.

Asymptotic studies of the flow in a rigid tube (Gill 1965; Corcos & Sellars 1959) have revealed that there are two types of high Reynolds number modes in a rigid tube where the vorticity is confined to thin regions near the centre of the tube or at the wall. The vorticity of the 'centre modes' is confined to a region of thickness $O(Re^{-1/4})$ at the centre of the tube, and the decay rate of these modes is $O(Re^{-1/2})$ smaller than the fluid strain rate. The vorticity of the 'wall modes' is confined to a layer of thickness $O(Re^{-1/3})$ at the wall, and the damping rate of these modes is $O(Re^{-1/3})$ smaller than the fluid strain rate. Both these modes are always stable. There have also been many numerical studies of the stability of parabolic pipe flow to axisymmetric and non-axisymmetric disturbances at finite Reynolds number (Davey & Drazin 1969; Garg & Rouleau 1972; Salwen & Grosch 1972). These have all concluded that the flow is stable to small disturbances at all Reynolds numbers, and there now appears to be a consensus that the flow in a rigid tube is stable to small-amplitude perturbations, but the observed instability may be due to perturbations of finite amplitude. This is supported by evidence that the flow in a tube can be maintained in the laminar state at Reynolds numbers much higher than the transition Reynolds number of 2300 if adequate precautions are taken to damp out vibrations in the system.

The stability characteristics of the wall modes were determined using asymptotic analysis in an earlier study (Kumaran 1998*b*). The configuration and the coordinate system used in the analysis are shown in figure 1. Perturbations of the form $v_i = \tilde{v}_i(r)\exp(\mathrm{i}kx + st)$ and $u_i = \tilde{u}_i(r)\exp(\mathrm{i}kx + st)$ were imposed, and the growth rate of

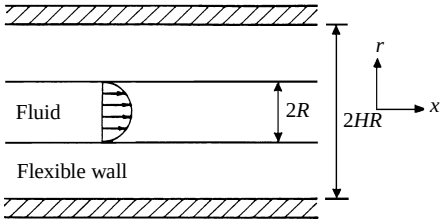

FIGURE 1. Configuration and definition of coordinate systems.

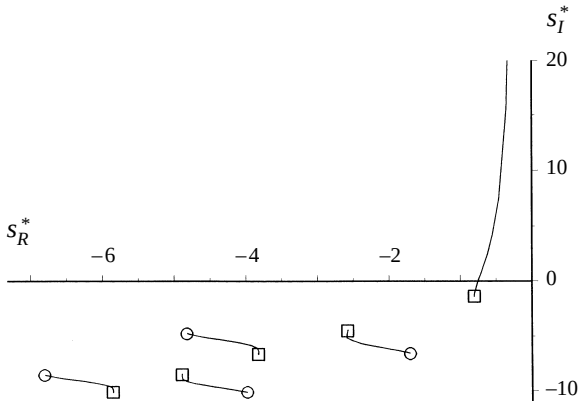

FIGURE 2. Solutions for the scaled growth rate $s^* = Re^{1/3}(sR/V)$ obtained in the asymptotic analysis of Kumaran (1998*b*). The circles are the roots in the limit $\Lambda^* \to \infty$, and the squares are the roots in the limit $\Lambda^* = 0$.

these perturbations s was determined as a function of the wavenumber k and the material and flow parameters. Since the vorticity of the wall modes is confined to a thin region near the wall of the tube, the wall elasticity has an effect on these modes. A scaling analysis showed that the elastic stresses in the wall affect the damping of the wall modes when the dimensionless number $\Lambda \equiv \epsilon^{-1/3}(G/\rho V^2)^{1/2} \sim 1$, where $\epsilon \equiv Re^{-1}$. It was shown, using scaling arguments, that the inertial and viscous stresses are of the same magnitude in the wall layer, and the parameter Λ represents the ratio of the elastic stresses in the wall material and the inertial (or viscous) stresses in the fluid. The velocity and stress fields were expanded in the small parameter ϵ, and an asymptotic analysis is used to determine the growth rate of the wall modes. In the regime $\Lambda \sim 1$, the elastic stress is large compared to the inertial stress in the wall material, and the wall admittance is only a function of the ratio of radii of the wall and the fluid H and the scaled wavenumber kR of the perturbations. There are multiple solutions for the scaled growth rate, $s^* = Re^{-1/3}(sR/V)$, which are shown in the complex plane in figure 2. In the limit $\Lambda \to \infty$, which corresponds to a rigid tube, the solutions (circles in figure 2) reported previously for a rigid tube are recovered. In the limit $\Lambda \to 0$, which is a wall with very small elasticity, the solutions converge to the squares shown in figure 2, and there is a smooth transition between these two in the intermediate regime. In addition, there is one mode in a flexible tube whose growth rate does not converge to any of the rigid tube modes, but which has a diverging frequency in the limit $\Lambda \to \infty$. This is the least-stable wall mode in a flexible tube, and its decay rate decreases proportional to $\Lambda^{-1/2}$ in the limit $\Lambda \to \infty$.

In § 2, the stability analysis for the least-stable wall mode is extended to the regime

$\Lambda \ll 1$ using a numerical scheme. It is observed that this mode becomes unstable when Λ is decreased below a transition value at a fixed Reynolds number, or when the Reynolds number is increased beyond a transition value at a fixed value of Λ. The neutral stability curves for this unstable mode are obtained using a continuation scheme, and the Reynolds number at which there is a transition from stable to unstable modes is determined as a function of the dimensionless parameter $\Sigma = (\rho G R^2/\eta^2)$, the ratio of radii H, the wavenumber kR, and the parameter η_r which is the ratio of viscosities of the wall material and the fluid.

2. Numerical analysis

In the present section, a numerical calculation used to determine the stability characteristics in the regime $\Lambda \ll 1$, where the asymptotic analysis is not expected to provide accurate results. Here, the parameter Λ is the ratio of the elastic stresses in the wall and the inertial or viscous stresses in the fluid. The numerical scheme, which is identical to that used in Kumaran (1998*a*), is briefly outlined here. The conservation equations for the velocity field in the fluid and the displacement field in the flexible wall are reduced to two fourth-order differential equations. There are two linearly independent solutions for the velocity field in the fluid which are consistent with the symmetry conditions at the centre of the tube. One of these is determined analytically, while the other is calculated using a fourth-order Runge–Kutta scheme with adaptive step size control. Since only one solution is determined numerically, an orthogonalization procedure is not necessary. There are two linearly independent solutions for the displacement field in the wall material which are consistent with the zero displacement conditions at $r = H$. Both of these are determined using a fourth-order Runge–Kutta technique using adaptive step size control, and an orthogonalization procedure is employed. The solutions for the fluid velocity and wall displacement fields at the interface are inserted into the boundary conditions to obtain the characteristic matrix. The characteristic equation, obtained by setting the determinant of this matrix to zero, is solved to determine the growth rate. The characteristic equation is a nonlinear equation, so it is not possible to determine the solutions analytically. In Kumaran (1998*a*), the solutions for the growth rate in the low Reynolds number regime were used as a starting guess, and an iterative Newton–Raphson scheme was used to obtain the growth rate at non-zero values of the Reynolds number. In the present analysis, the same iterative scheme is used, but the solution for the growth rate obtained from the asymptotic analysis for the wall modes (Kumaran 1998*b*) is used as the starting guess.

In Kumaran (1998*a*), the consistency of the numerical scheme was verified in three ways. In the limits of low and high Reynolds number, it was found that the numerical results were in agreement with the low and high Reynolds number analyses of Kumaran (1995*a*, *b*). In addition, the numerical results were compared with the results of Davey & Drazin (1969) for the Poiseuille flow in a rigid tube, and it was shown that the results of the numerical scheme converge to those of Davey & Drazin in the limit where $G \to \infty$ (infinite elasticity) and in the limit $H \to 0$ where the thickness of the wall is small compared with the radius of the tube. In the present section, the numerical results are compared with the high Reynolds number asymptotic analysis for the wall modes given in Kumaran (1998*b*). The scaled growth rate in the asymptotic analysis, $s^* = Re^{1/3}(sR/V)$, depends on a dimensionless parameter $\Lambda^* = (2kR)^{1/3}\Lambda C(kR, H)/4$, where $C(kR, H)$ is the inverse of the admittance, kR is a dimensionless wavenumber and $\Lambda = Re^{1/3}(G/\rho V^2)$. The

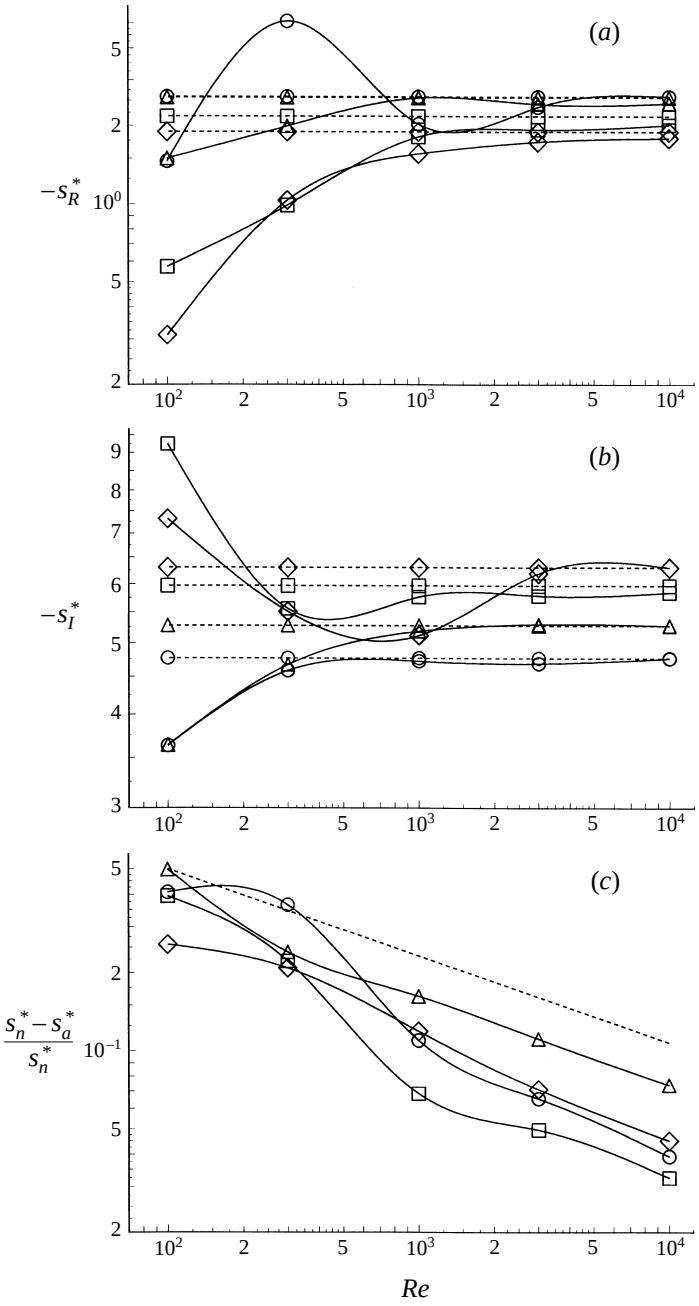

FIGURE 3. Comparison of the numerical s_n^* and asymptotic s_a^* results for (*a*) the real part of the growth rate s_R^*, (*b*) the imaginary part of the growth rate s_I^*, (*c*) the ratio $|s_n^* - s_a^*|/|s_n^*|$ for the wall mode with the second lowest damping rate. In (*a*) and (*b*), the solid lines are the numerical results and the broken lines are the asymptotic results. In (*c*), the broken line has a slope of $(-1/3)$. The dimensionless wavenumber $kR = 1$, the ratio of radii $H = 2$, and $\Lambda^* = 2.4172\Lambda$ for these values of H and kR. The parameter values are ○, $\Lambda = 0.1$; △, $\Lambda = 0.3$; □, $\Lambda = 1.0$; ◇, $\Lambda = 1.0$.

parameter Λ^* is proportional to the normal stress in the wall material (scaled by ρV^2) and the normal displacement (scaled by R). The asymptotic analysis indicates that the wall mode with the lowest damping rate has a diverging frequency for $\Lambda^* \gg 1$; the numerical results for this mode are examined a little later. Here, the wall mode with the second lowest damping rate, which has a finite frequency at all values of Λ^*, is chosen for the validation of the numerical code. A comparison for the real and imaginary parts of the numerically evaluated growth

rate s_n^* and the asymptotic value of the growth rate s_a^* in the high Reynolds number limit are given in figures 3(a) and 3(b). Here, the wavenumber $kR = 1$, and four different values of the dimensionless parameter Λ are considered. It is seen that there is very good agreement between the numerical and analytical solutions at Reynolds numbers between 1000 and 10 000, even though $Re^{-1/3}$ is not very small at these values of Re. It is interesting to note that a similar observation was made by Davey & Drazin (1969) when they compared their numerical results for wall modes in a rigid tube with the asymptotic results of Corcos & Sellars (1959). The relative difference between the numerical and asymptotic growth rates, $(|s_n^* - s_a^*|/|s_n^*|)$, is shown in figure 3($c$). Here, it can be seen that the asymptotic solution is in error by $O(Re^{-1/3})$, in agreement with the prediction of the asymptotic analysis. Consequently, the present numerical scheme is consistent with the asymptotic analysis in Kumaran (1998b).

The variation in the real and imaginary parts of the growth rate for the least-stable mode, which has a diverging frequency in the rigid tube limit, is shown in figures 4(a) and 4(b). The broken line shows the asymptotic results of Kumaran (1998b) for $kR = 1$, and different values of Λ^*, while the solid lines show the results of the numerical calculation for $H = 2$, $\eta_r = 0$ and for different values of the Reynolds number. It can be seen that there is good agreement between the asymptotic and numerical results for $\Lambda^* \sim 1$, but the agreement is poor for $\Lambda^* \gg 1$ and $\Lambda^* \ll 1$. There are significant differences between the asymptotic and numerical results for $\Lambda^* \gg 1$ because the frequency of oscillations becomes large in this regime, and the inertial effects in the wall, which have been neglected in the asymptotic analysis are no longer negligible. In addition, it is also observed that the growth rate deviates significantly from the asymptotic value for $\Lambda^* \ll 1$, and the perturbations become unstable in the range $0.01 \leqslant \Lambda^* \leqslant 0.1$ for Reynolds numbers from 1000 to 10 000. The stability of this mode at intermediate Reynolds number is analysed in the present section using the numerical scheme discussed above.

The neutral stability curves for the least-stable wall mode are determined using an analytic continuation technique, and the parameter values for the neutrally stable perturbations obtained as discussed above are used as the starting guess. The Reynolds number for the neutrally stable modes is determined as a function of the dimensionless parameter $\Sigma = (\rho G R^2/\eta^2)$. The parameter Σ is chosen as the independent variable because it is independent of the fluid velocity, and is dependent only on the fluid and wall parameters, and the results are expressed in terms of the parameter Σ to facilitate comparison with the previous results of Kumaran (1998a). The Reynolds number for neutrally stable modes depends on the wavenumber kR, the ratio of wall and fluid radii H and the ratio of viscosities η_r. In this section, the results for $\eta_r = 0$ are first analysed, and then the effect of variation in η_r on the neutrally stable modes is determined.

2.1. *Results for* $\eta_r = 0$

The Reynolds number for neutrally stable modes is shown as a function of Σ for $1 \leqslant \Sigma \leqslant 10^5$ for different values of H and kR in figures 5 and 6. In the limit

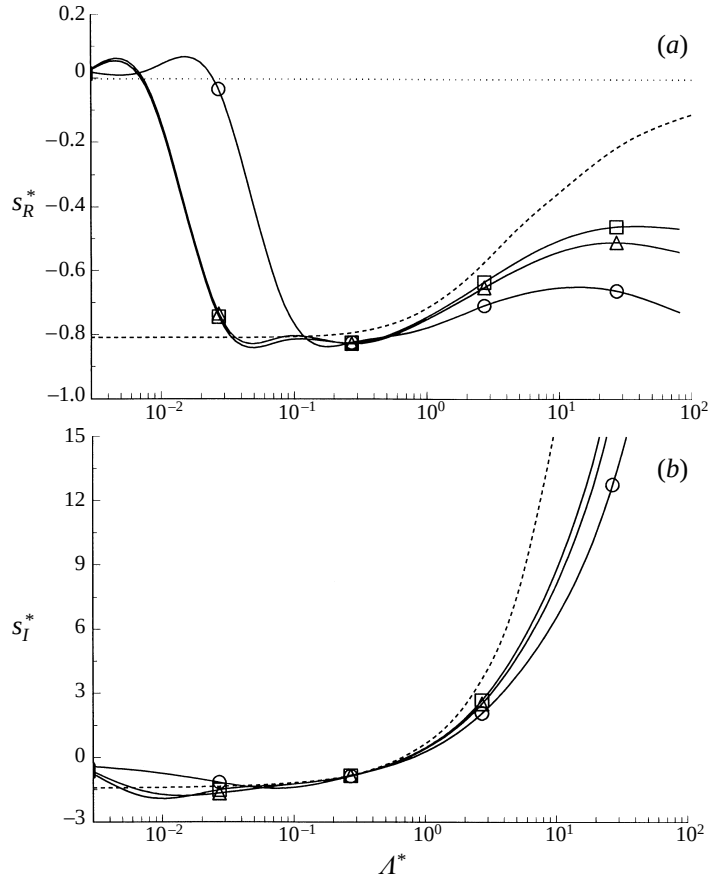

FIGURE 4. Comparison of the asymptotic and numerical results for (*a*) the real part, (*b*) the imaginary part of the growth rate for the wall mode with the lowest damping rate at wavenumber $kR = 1$, ratio of radii $H = 2$ and ratio of viscosities $\eta_r = 0$. The broken line shows the asymptotic results, while the parameter values for the numerical results are ○, $Re = 10^3$; △, $Re = 5 \times 10^3$ and □, $Re = 10^4$. The dotted line in (*a*) represents $s_R^* = 0$.

$\Sigma \ll 1$, the Reynolds number decreases proportional to $\Sigma^{1/2}$. This is in contrast to the viscous modes (Kumaran 1995*a*), where the Reynolds number decreases proportional to Σ, indicating that the neutrally stable modes obtained in the present analysis are distinct from the neutrally stable wall modes obtained in Kumaran (1995*a*). Figure 5 shows that neutral stability curves could have a rather complex behaviour in the intermediate Reynolds number regime for certain values of kR and H, with the possibility of turning points and isolated domains of unstable perturbations. However, for other values of kR and H, the neutral curves are monotonic, and do not show isolated regions of instability, as illustrated in figure 6.

The critical Reynolds number, which is the minimum Reynolds number at which there are neutrally stable modes for a specified value of H, is shown as a function of Σ in figure 7(*a*). The critical Reynolds number increases with an increase in Σ, and has a behaviour of the type Σ^{α} in the limit $\Sigma \gg 1$, where α varies between 0.7 and 0.75. This behaviour is similar to that of the neutral stability curves analysed in Kumaran (1998*a*) for the continuation of the viscous modes. Moreover, it is observed that the critical Reynolds number exhibits the possibility of discontinuities. This is

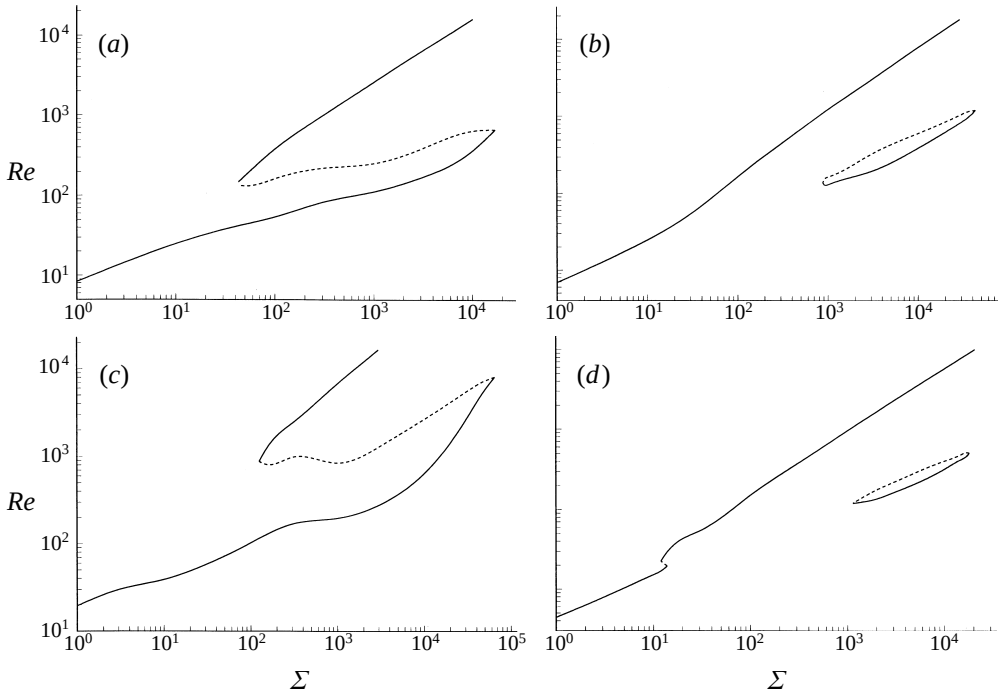

FIGURE 5. Neutral stability curves in the (Σ, Re)-plane for the wall mode with the lowest damping rate. The parameter values are (*a*) $H = 2.0, kR = 1.0$; (*b*) $H = 2.0, kR = 2.0$; (*c*) $H = 1.5, kR = 1.0$; (*d*) $H = 3.0, kR = 1.0$. The solid lines indicate a transition from stable to unstable modes when the Reynolds number is increased, and the broken lines indicate a transition from unstable to stable modes when the Reynolds number is increased.

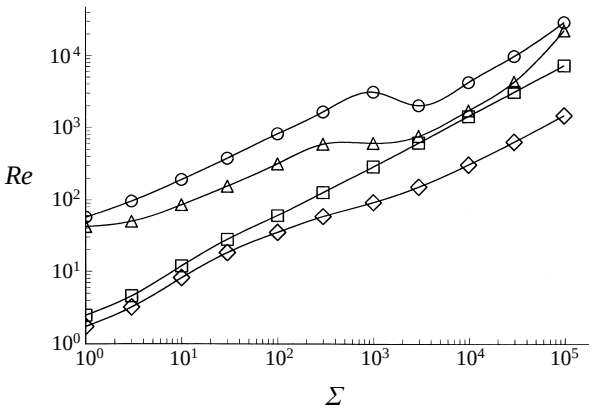

FIGURE 6. Neutral stability curves in the (Σ, Re)-plane for the wall mode with the lowest damping rate. The parameter values are ○, $H = 1.1, kR = 1.0$; △, $H = 1.2, kR = 1.0$; □, $H = 5.0, kR = 1.0$; ◇, $H = 10.0, kR = 1.0$.

due to the presence of turning points and isolated domains of instability in the neutral stability curves in the (Re, Σ)-plane discussed earlier. A comparison of the critical Reynolds number for the wall modes analysed here and the viscous modes that were analysed in Kumaran (1998) is also shown in figure 7(*a*). It is seen that at $H = 10$, the viscous modes have a lower critical Reynolds number for $1 \leqslant \Sigma \leqslant 10^5$, but for

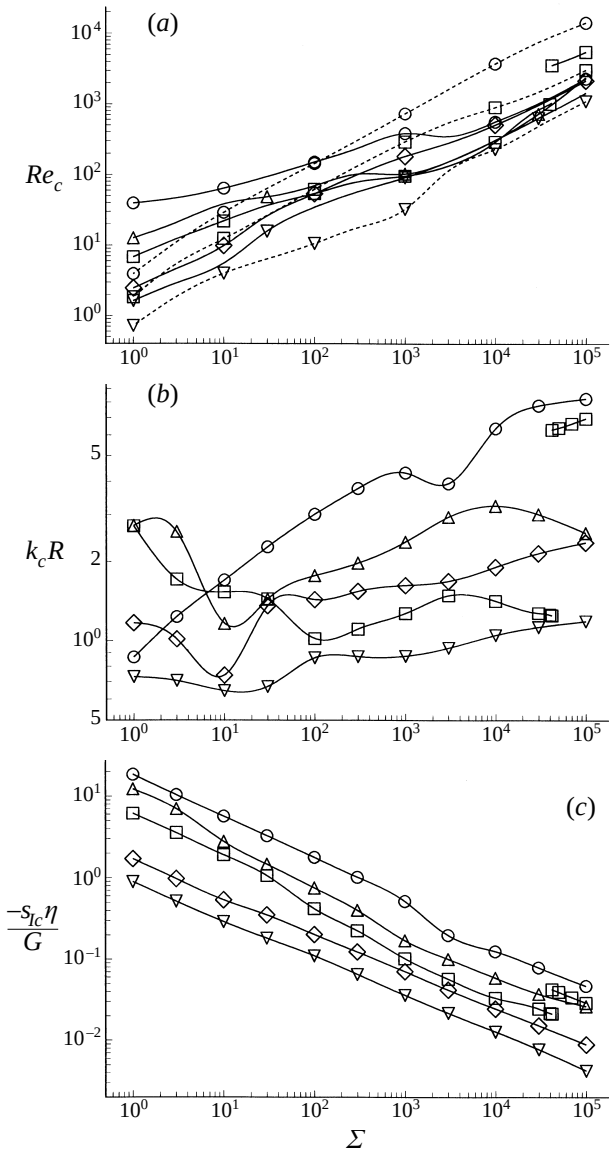

FIGURE 7. The critical Reynolds number (*a*), non-dimensional wavenumber of the neutrally stable mode (*b*) and non-dimensional frequency of the neutrally stable mode (*c*) as a function of Σ. $\circ$, $H = 1.2$; $\triangle$, $H = 1.5$; $\square$, $H = 2.0$; $\diamond$, $H = 5.0$; ∇, $H = 10.0$. In (*a*), the solid lines give the critical Reynolds number for the wall modes and the broken lines give the critical Reynolds number for the viscous modes.

$H = 2$ and $H = 1.2$, the wall modes have a lower critical Reynolds number for $10^2 \leqslant \Sigma \leqslant 10^5$. The discontinuity in the critical Reynolds number for $H = 1.2$ is due to the disappearance of isolated domains of instability (shown in figure 5*b*, *d*) at the value of Σ where the curve is discontinuous. The wavenumber of the neutrally stable mode, scaled by the inverse of the tube radius, is shown as a function of Σ in figure 7(*b*), and the frequency of the neutrally stable mode scaled by (G/η) is shown as a function of Σ in figure 7(*c*). It is useful to note that the frequency of the

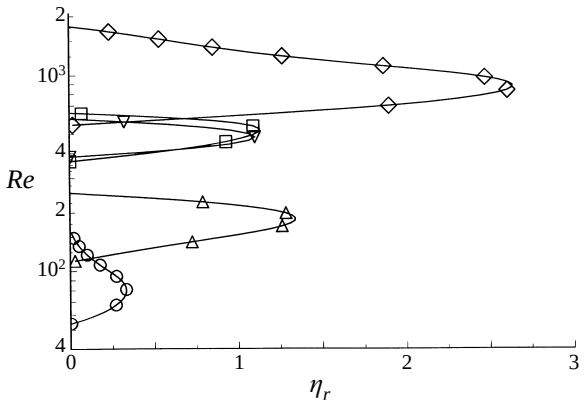

FIGURE 8. The neutral stability curves in the (η_r, Re)-plane for $H = 2$. ○, $\Sigma = 10^2, kR = 1.0$; △, $\Sigma = 10^3, kR = 1.0$; □, $\Sigma = 10^4, kR = 1.0$; ◇, $\Sigma = 10^4, kR = 0.5$; ∇, $\Sigma = 10^4, kR = 2.0$.

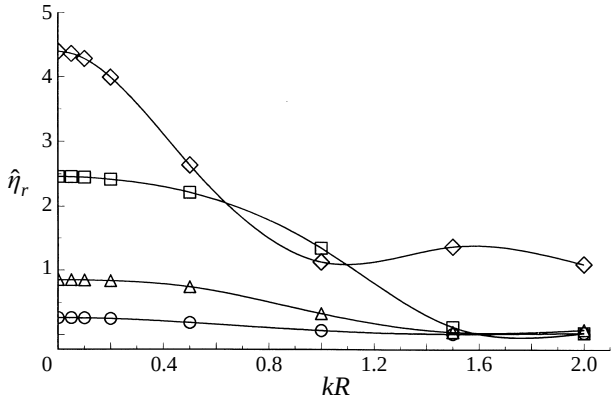

FIGURE 9. The maximum value of ratio of viscosities $\hat{\eta}_r$ at which there are neutrally stable modes at a specific wavenumber as a function of the scaled wavenumber (kR) at $H = 2$. ○, $\Sigma = 10$; △, $\Sigma = 10^2$; □, $\Sigma = 10^3$; ◇, $\Sigma = 10^4$.

neutrally stable mode is negative, indicating that the phase velocity of the neutrally stable perturbations is always opposite to the direction of flow.

2.2. *Results for* $\eta_r > 0$

The effect of variation in the ratio of viscosities η_r on the Reynolds number of neutrally stable modes is shown in figure 8. It is observed that as the ratio of viscosities for the neutrally stable modes increases, the Reynolds number for transiton from stable to unstable perturbations increases from $\eta_r = 0$, undergoes a turning point and then decreases to zero at a finite Reynolds number. This behaviour was observed at all values of H, Σ and kR studied here, and the more complex behaviour reported in Kumaran (1998*a*) for the viscous modes is not observed in the present case. Figure 8 indicates that there is a finite region in the (Re, η_r)-plane where there are unstable modes, and there is a maximum ratio of viscosities $\hat{\eta}_r$ for a specified H and kR where neutrally stable modes can exist. This maximum ratio of viscosities is shown as a function of the scaled wavenumber (kR) in figure 9 for $H = 2$ and for different values of Σ. It is observed that $\hat{\eta}_r$ shows a maximum at $kR = 0$, and decreases as kR is increased. This trend was observed for all the values of Σ analysed here.

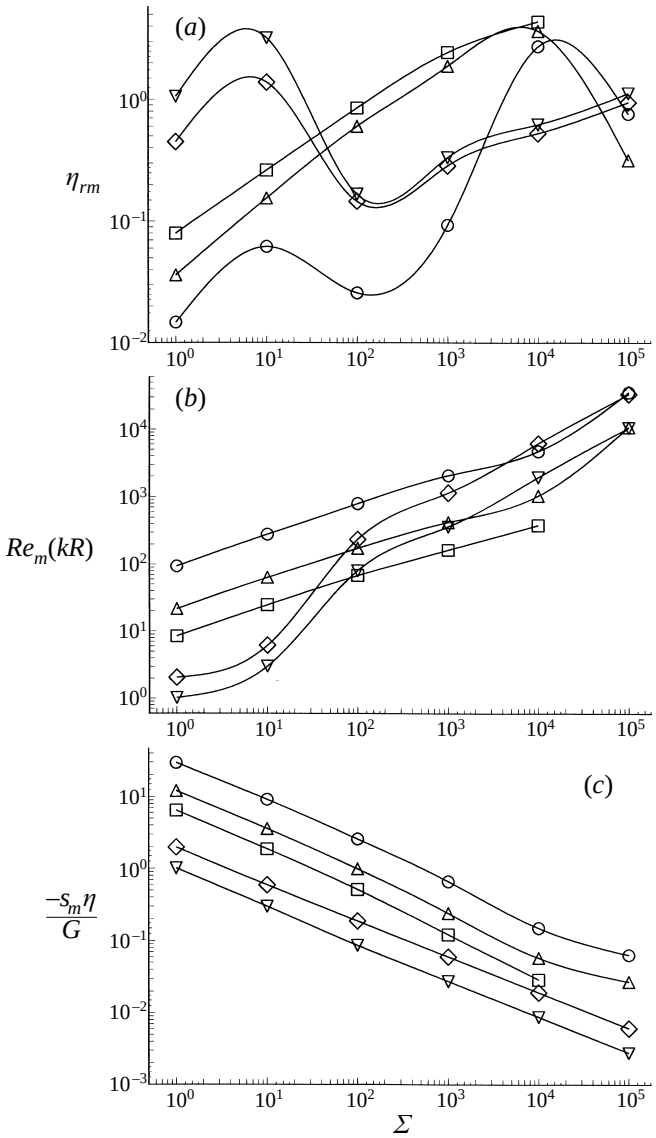

FIGURE 10. The maximum ratio of viscosities η_{rm} at which there are neutrally stable modes in the limit $(kR) \to 0$ (*a*); the product of the Reynolds number and the non-dimensional wave number for the neutrally stable modes (*b*); and the scaled frequency of the neutrally stable modes (*c*) as a function of Σ. $\circ$, $H = 1.2$; $\triangle$, $H = 1.5$; $\square$, $H = 2.0$; $\diamond$, $H = 5.0$ and ∇, $H = 10.0$.

The maximum of the $\hat{\eta}_r, (kR)$ curve at $kR = 0$, denoted η_{rm}, represents the maximum value of the ratio of viscosities at which unstable modes can be present at any wavenumber for a specified value of H. Therefore, η_{rm} represents a global stability limit, and perturbations are always stable for $\eta_r > \eta_{rm}$. This maximum value is shown as a function of Σ for different values of H in figure 10(*a*). It is observed that η_{rm} tends to increase as Σ increases, though there is a decrease when Σ increases beyond 10^4. The numerical calculations indicate that the critical Reynolds number Re_m of the neutrally stable modes at $\eta_r = \eta_{rm}$ increases proportional to $(kR)^{-1}$ in the limit $(kR) \to 0$. The product $(kR)Re_m$ is shown as a function of Σ in figure 10(*b*). It is

observed that the critical Reynolds number increases with Σ, but the dependence on H is non-monotonic. The numerical calculations indicate that this is due to the presence of turning points and isolated domains of instability with a much lower critical Reynolds number for H between 1.5 and 3.0, and the absence of these for H less than 1.2 and greater than 5.0. The non-dimensional frequency of the neutrally stable modes at $\eta_r = \eta_{rm}$, shown as a function of Σ in figure 10(*c*), shows a monotonic decrease as Σ is increased.

3. Discussion and conclusions

The stability of wall modes in the limit of high Reynolds number was earlier determined using asymptotic analysis (Kumaran 1998*b*) for the regime $\Lambda^* \sim 1$, where $\Lambda^* \equiv (kR)^{1/3}\Lambda C(kR, H)$ is a dimensionless parameter in the asymptotic analysis, $\Lambda \equiv Re^{1/3}(G/\rho V^2)$ and $C(kR, H)$ is the inverse of the wall admittance. The results have been extended to the intermediate Reynolds number regime using numerical calculations in the present study. The variation in the decay rate of the least-stable wall mode in the regime $\Lambda^* \ll 1$ was determined numerically, and it was found that this mode becomes unstable when Λ^* decreases below a critical value at a fixed Reynolds number, or when the Reynolds number increases beyond a critical value at a fixed Λ^*. The neutral stability curves for this mode were determined as a function of the parameter $\Sigma = (\rho G R^2/\eta^2)$, the wavenumber kR, ratio of radii H, and the ratio of viscosities of the wall and the fluid η_r. The critical Reynolds number increases proportional to $\Sigma^{1/2}$ in the limit $\Sigma \ll 1$, and increases proportional to Σ^{α}, where $0.7 \leqslant \alpha \leqslant 0.75$, in the limit $\Sigma \gg 1$. In the intermediate regime, the neutral stability curves have a complex behaviour with the possibility of turning points and isolated regions of unstable modes. The dependence of the Reynolds number of neutrally stable modes on the ratio of viscosities η_r is complex, and it is found that the Reynolds number first increases as η_r is increased from zero and undergoes a turning point, and any further increase in Reynolds number leads to a decrease in the ratio of viscosities for the neutral modes. At a specified value of Σ, there is the possibility of neutrally stable modes only if the ratio of viscosities is less than a maximum value η_{rm}; perturbations are always stable for $\eta_r > \eta_{rm}$.

An energy balance analysis similar to that of Kumaran (1995*b*) can be used to understand the physical mechanism leading to the instability. A balance for the total energy of the fluctuations can be written as

$$\frac{\mathrm{d}\mathscr{E}}{\mathrm{d}t} = \mathscr{C} + \mathscr{S} - \mathscr{D}_f - \mathscr{D}_w, \tag{3.1}$$

where $\mathscr{E}$ is the energy of the fluctuations, $\mathscr{C}$ is the rate of transfer of energy from the mean flow to the fluctuations due to the convective terms in the momentum equation, $\mathscr{S}$ is the transfer of energy due to the work done by the mean flow at the interface, and $\mathscr{D}_f$ and $\mathscr{D}_w$ are the rates of dissipation of energy due to viscous effects in the fluid and the wall. The convective transport of energy $\mathscr{C}$ is zero in the leading approximation because the tangential and normal velocities in the fluid are out of phase by an angle of $(\pi/2)$ (Kumaran 1995*b*). Thus, there is an instability when the energy transfer rate $\mathscr{S}$ is larger than the rate of dissipation $\mathscr{D}_f + \mathscr{D}_w$. The rate of transport due to the work done by the mean flow at the interface is (Kumaran 1995*b*)

$$\mathscr{S} = 2\pi R \int \mathrm{d}x\, \tau_{xr}(v_x - \partial_t u_x)|_{r=R}. \tag{3.2}$$

The rate of dissipation of energy in the fluid is

$$\mathscr{D}_f = 2\pi R\eta \int \mathrm{d}x \int_0^R r\,\mathrm{d}r\,\tau_{xr}(\partial_r v_x + \partial_x v_r). \tag{3.3}$$

From the scaling of the spatial and velocity coordinates in equations in Kumaran (1998*b*), it can be inferred that the tangential velocity v_x is large compared to the normal velocity in the wall layer. In addition, the tangential velocity v_x is also large compared to the rate of change of normal displacement $\partial_t u_x$ in (3.2). With these simplifications, $\mathscr{S}$ can be expressed in terms of the Fourier components of the scaled velocities $\tilde{v}_r^*$ and $\tilde{v}_x^*$:

$$\mathscr{S} = (Re^{1/3}2\pi R\eta V^2)\exp[(s^* + \bar{s^*})] \int \mathrm{d}k[\bar{\tilde{v}_x^*} d_{z^*}\tilde{v}_x^* + \tilde{v}_x^* d_{z^*}\bar{\tilde{v}_x^*}]|_{r^*=1} \tag{3.4}$$

where the overbar denotes the complex conjugate, $\tilde{v}_x^* = \tilde{v}_x/V$, $\tilde{v}_r^* = Re^{1/3}\tilde{v}_r/V$, $s^* = Re^{1/3}(sR/V)$ and $z^* = Re^{1/3}(1-r)$. The rate of dissipation of energy in the fluid can be expressed in a similar fashion:

$$\mathscr{D}_f = (Re^{1/3}2\pi R\eta V^2)\exp[(s^* + \bar{s^*})] \int \mathrm{d}k \int_0^\infty \mathrm{d}z^*[2(d_{z^*}\tilde{v}_x^*)(d_{z^*}\bar{\tilde{v}_x^*})]. \tag{3.5}$$

In the above expression, the lower limit $z^* = 0$ corresponds to the wall of the tube, while the upper limit $z^* = Re^{1/3}$ at the centre of the tube has been approximated by $z^* = \infty$ in the limit $Re \gg 1$. The difference $\mathscr{S} - \mathscr{D}_f$ reduces to

$$\mathscr{S} - \mathscr{D}_f = (Re^{1/3}2\pi R\eta V^2)\exp[(s^* + \bar{s^*})] \int \mathrm{d}k \int_0^\infty \mathrm{d}z^*[(\bar{\tilde{v}_x^*} d_{z^*}^2\tilde{v}_x^*) + (\tilde{v}_x^* d_{z^*}^2\bar{\tilde{v}_x^*})]. \tag{3.6}$$

For a non-dissipative wall ($\eta_r = 0$), a transition from stable to unstable modes could be expected when $\mathscr{S} - \mathscr{D}_f$ goes from negative to positive. Consequently, the instability results when the transfer of energy from the mean flow to the fluctuations due to the shear work done by the mean flow at the interface is greater than the dissipation of energy due to viscous effects. This energy balance indicates that the present instability is distinct from the Tollmien–Schlichting modes, because in the Tollmien–Schlichting modes the instability is caused by the transport of energy from the mean flow to the fluctuations in a viscous critical layer in the fluid of thickness $Re^{-1/3}$ smaller than the tube radius. The absence of this critical layer indicates that the present instability is not a Tollmien–Schlichting instability.

The instability obtained in the present analysis is not a continuation of the wall modes in a rigid tube, because the mode that becomes unstable corresponds to a wall mode in a flexible tube which does not converge to any of the wall modes in a rigid tube, but has a diverging frequency in the limit of a rigid tube. Consequently, this instability cannot be classified as the continuation of a Tollmien–Schlichting instability in a rigid tube, and it is appropriate to classify it as a flow-induced surface instability which can exist only in the presence of wall flexibility, in the classification of Carpenter & Garrad (1985). In the classification system developed by Benjamin (1963), the wall modes come under the category of Class B modes. This is because from figure 8 it is observed that an increase in the wall dissipation increases the Reynolds number of neutrally stable modes. Moreover, from figure 5(*a*), it is seen that the (Re, Σ)-curve could have three points where the flow could be neutrally stable. As η_{rm} is increased, the lower branch moves upward indicating that an increase in viscosity increases the Reynolds number at which the transition to unstable modes takes place.

The critical Reynolds number for the present instability is compared with those for the continuation of the viscous modes (Kumaran 1998*a*) in the intermediate Reynolds number regime in figure 7(*a*). It is observed that the critical Reynolds number for the present instability is greater than that for the continuation of the viscous mode for $H = 10.0$, but for $H = 1.2$ and $H = 2.0$, there are ranges of Σ where the present instability has a lower critical Reynolds number than the continuation of the viscous mode. This implies that at higher values of H where the wall thickness is large compared to the tube radius, the continuation of the viscous mode is the most unstable mode, while at lower values of H, the continuation of the wall mode analysed here is more unstable over certain ranges of the parameter Σ. Moreover, the critical Reynolds number is a non-monotonic function of H for certain values of Σ, first decreasing and then increasing as H is increased. This is because it exhibits the type of behaviour shown in figure 5 at lower values of H, where the neutral stability curve is not monotonic but has turning points and sometimes isolated domains of instability, where the Reynolds number for the transition from stable to unstable modes for the lower branch is considerably lower than that for the upper branches of the neutral stability curves. This feature is not observed at higher values of H, and consequently the critical Reynolds number could show an increase as H is increased.

The Reynolds number for the neutrally stable modes has a complex dependence on the ratio of viscosities η_r, as reported in the previous section. As the ratio of viscosities is increased, the Reynolds number of neutral modes initially increases, and then there is a turning point in the Re, η_r curve and a further increase in the Reynolds number causes a decrease in the ratio of viscosities η_r. Moreover, the ratio of viscosities decreases to $\eta_r = 0$ at a finite Reynolds number, indicating that there is a finite region in the (η_r, Re_n)-plane where the perturbations are unstable. However, the more complex types of behaviour reported in Kumaran (1998*a*) for the continuation of the viscous modes, where there is the possibility of the Reynolds number of neutral modes decreasing as the ratio of viscosities is increased, are not observed here. There is a maximum ratio of viscosities η_{rm} for a specified H at which neutrally stable modes can exist; perturbations are always stable for $\eta_r > \eta_{rm}$. The maximum ratio of viscosities varies between 0.01 and 1.0 for $1 \leqslant \Sigma \leqslant 10^4$; this is of the same magnitude as that reported for the continuation of the viscous modes in Kumaran (1998*a*). The critical Reynolds number for the continuation of the viscous modes was compared with the experimental results of Krindel & Silberberg (1979) for the flow in a gel-walled tube in Kumaran (1998*a*), and it was reported that the anomalous drag forces observed in that experiment could be due to an instability that is a continuation of the viscous modes. The present analysis indicates that the continuation of the viscous mode is more unstable than the continuation of the wall mode in the regime $10 \leqslant H \leqslant 30$, appropriate for the experiments of Krindel & Silberberg, and so the continuation of the viscous mode is the most unstable mode in this regime. However, for lower values of H, the continuation of the wall mode could be more unstable, and the results of the present analysis would be relevant in this regime.

The author would like to thank the Department of Science and Technology, Government of India for financial support.

REFERENCES

Benjamin, T. B. 1963 The threefold classification of unstable disturbances in flexible surfaces bounding inviscid flows. *J. Fluid Mech.* **16**, 436–450.

Carpenter, P. W. & A. D. Garrad 1985 The hydrodynamic stability of flows over Kramer-type compliant surfaces. Part 1. Tollmien–Schlichting instabilities. *J. Fluid Mech.* **155**, 465–510.

Corcos, G. M. & Sellars, J. R. 1959 On the stability of fully developed pipe flow. *J. Fluid Mech.* **5**, 97–112.

Davey, A. & Drazin, P. G. 1969 The stability of Poiseuille flow in a pipe. *J. Fluid Mech.* **36**, 209–218.

Garg, V. K. & Rouleau, W. T. 1972 Linear spatial stability of pipe Poiseuille flow. *J. Fluid Mech.* **54**, 113–127.

Gill, A. E. 1965 On the behaviour of small disturbances to Poiseuille flow in a circular pipe. *J. Fluid Mech.* **21**, 145–172.

Krindel, P. & Silberberg, A. 1979 Flow through gel-walled tubes. *J. Colloid Interface Sci.* **71**, 34–50.

Kumaran, V. 1995*a* Stability of the viscous flow of a fluid through a flexible tube. *J. Fluid Mech.* **294**, 259–281.

Kumaran, V. 1995*b* Stability of the flow of a fluid through a flexible tube at high Reynolds number. *J. Fluid Mech.* **302**, 117–139.

Kumaran, V. 1998*a* Stability of fluid flow in a flexible tube at intermediate Reynolds number. *J. Fluid Mech.* **357**, 123–140.

Kumaran, V. 1998*b* Asymptotic analysis of wall modes in a flexible tube. *Euro. Phys. J.* B (submitted).

Salwen, H. & Grosch, C. E. 1972 The stability of Poiseuille flow in a pipe of circular cross section. *J. Fluid Mech.* **54**, 93–112.